

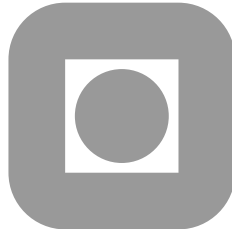
NORGES TEKNISK-NATURVITENSKAPELIGE
UNIVERSITET

Error estimates in inverse electromagnetic scattering

by

Larisa Beilina, Marte P. Hatlo, Harald E. Krogstad

PREPRINT
NUMERICS NO. 10/2007



NORWEGIAN UNIVERSITY OF
SCIENCE AND TECHNOLOGY
TRONDHEIM, NORWAY

This report has URL
<http://www.math.ntnu.no/preprint/numerics/2007/N10-2007.pdf>
Address: Department of Mathematical Sciences, Norwegian University of Science and
Technology, N-7491 Trondheim, Norway.

Error estimates in inverse electromagnetic scattering

Larisa Beilina, Marte P. Hatlo, Harald E. Krogstad

December 19, 2007

In this paper we derive an a posteriori error estimate and present two different adaptive algorithms for an inverse electromagnetic scattering problem.

The inverse problem is formulated as an optimal control problem, where we solve equations expressing stationarity of an associated Lagrangian. The a posteriori error estimate for the Lagrangian couples residuals of the computed solution to weights of the reconstruction. We show that the weights can be obtained by solving an associated linearized problem for the Hessian of the Lagrangian, which is used in the second algorithm, while in the first algorithm we compute only the residuals. The performance of the adaptive finite element method and the usefulness of the a posteriori error estimate are illustrated in numerical examples.

1 Introduction

We apply the mesh-adaptive method, developed in [3], to an inverse electromagnetic scattering problem. The method is based on an a posteriori error estimate which couples residuals of the computed solution to weights in the reconstruction. The new element in the present work is the introduction of absorbing and mirror boundary conditions in the formulation of the forward problem. Thus, the a posteriori error estimate for the inverse problem is also new. The derivation of the a posteriori estimate for the error in the Lagrangian follows the main approach to adaptive error control in computational differential equations, presented in [2, 7] and references therein.

The inverse problem consists of reconstructing the unknown material variable, that is, the dielectric permittivity, $\epsilon(x)$, from data measured on parts of the surface of the given domain, given the wave input on other parts. By solving the wave equation with the same input, the material variables are in principle obtained by fitting the computed solution to the measured data. The problem is formulated as finding a stationary point of the Lagrangian, involving the forward wave equation (the state equation), the backward wave equation (the adjoint equation), and an equation expressing that the gradient with respect to the parameter vanishes. The optimum is found in an iterative process solving the forward and backward wave equations and updating the material coefficient for each step.

We present two different adaptive algorithms to solve the inverse problem. In the first algorithm, the space-mesh adaptivity is based only on the computation of the residuals, since they already give us enough information. The second algorithm is extended to include computations of the weights. To compute the weights, we propose to solve a linearized problem for the Hessian of the Lagrangian.

Finally, numerical experiments where a periodic structure is reconstructed, show the possibilities of using adaptive error control in computational inverse scattering.

2 Mathematical model

We shall restrict ourselves to the propagation of light in a mixed dielectric medium in a bounded domain $\Omega \subset \mathbb{R}^d$, $d = 2, 3$, with boundary Γ , governed by Maxwell's equations:

$$\begin{aligned} \frac{\partial D}{\partial t} - \nabla \times H &= -J, & \text{in } \Omega \times (0, T], \\ \frac{\partial B}{\partial t} + \nabla \times E &= 0, & \text{in } \Omega \times (0, T], \\ \nabla \cdot D &= \rho, & \text{in } \Omega \times (0, T], \\ \nabla \cdot B &= 0, & \text{in } \Omega \times (0, T]. \end{aligned} \quad (1)$$

Here $E(x, t)$ and $H(x, t)$ are the electric and magnetic fields, whereas $D(x, t)$ and $B(x, t)$ are the electric and magnetic inductions, respectively. We assume that the dielectric permittivity, $\epsilon(x)$, is scalar and that the material is non-magnetic, so that $\mu(x) = 1$. Then $D = \epsilon E$ and $B = H$. The current density, J , and charge density, ρ , are both assumed to be zero.

By eliminating B and D from (1) we obtain two independent partial differential equations

$$\begin{aligned} \epsilon \frac{\partial^2 E}{\partial t^2} + \nabla \times (\nabla \times E) &= 0, \\ \frac{\partial^2 H}{\partial t^2} + \nabla \times (\epsilon^{-1} \nabla \times H) &= 0, \end{aligned} \quad (2)$$

which may be solved imposing appropriate initial and boundary conditions.

For simplicity, we only consider the problem in terms of $E(x, t)$. Taking into account the vector identity $\nabla \times \nabla \times V = \nabla(\nabla \cdot V) - \Delta V$, we obtain

$$\epsilon \frac{\partial^2 E}{\partial t^2} - \nabla \cdot (\nabla E) = 0, \quad \text{in } \Omega \times (0, T]. \quad (3)$$

A similar equation is valid for H .

Let $\Gamma_1 \cup \Gamma_2 \subset \Gamma$ and $\Gamma_3 = \Gamma \setminus \Gamma_1 \cup \Gamma_2$, and consider the forward problem consisting of (3) and the following initial and boundary conditions (Here and below, we denote $Dv = \frac{\partial v}{\partial t}$)

$$\begin{aligned} E(\cdot, 0) &= 0, \quad \frac{\partial E}{\partial t}(\cdot, 0) = 0, & \text{in } \Omega, \\ \partial_n E|_{\Gamma_1} &= v_1, & \text{on } \Gamma_1 \times (0, t_1], \\ \partial_n E|_{\Gamma_1} &= DE, & \text{on } \Gamma_1 \times (t_1, T], \\ \partial_n E|_{\Gamma_2} &= DE, & \text{on } \Gamma_2 \times (0, T], \\ \partial_n E|_{\Gamma_3} &= 0, & \text{on } \Gamma_3 \times (0, T], \end{aligned} \quad (4)$$

Here v_1 is a pulse emitted from Γ_1 , which propagates into Ω until $t = t_1$. We use first order absorbing boundary conditions, given in [6], on $\Gamma_1 \times (t_1, T]$ and $\Gamma_2 \times (0, T]$. At the lateral boundaries Γ_3 we use mirror boundary conditions.

Our goal is to solve the inverse problem for (3) and (4), or to find the material parameter $\epsilon(x)$ from data at a finite set of observation points on Γ . The data are generated in experiments where pulses are emitted from Γ_1 , backscattered by the material inhomogeneities, and recorded on parts of the boundary Γ .

In this paper, data are generated by computing the forward problem (3) and (4) for given values of the parameters, and saving the solution on parts of the boundary. The coefficients are then “forgotten” and the goal is to reconstruct the coefficients from the computed boundary data.

3 A hybrid finite element/difference method

To solve equation (3)-(4) we use a hybrid FEM/FDM method developed in [5]. The method uses continuous, piecewise linear finite elements in space and time on a partially structured mesh in space. The computational space domain Ω is decomposed into a finite element domain Ω_{FEM} , with an unstructured mesh, and a finite difference domain Ω_{FDM} , with a structured mesh. Typically, Ω_{FEM} covers only a small part of Ω . In Ω_{FDM} we use quadrilateral elements in \mathbb{R}^2 and hexahedra in \mathbb{R}^3 . In Ω_{FEM} we use a finite element mesh $K_h = \{K\}$ with elements K consisting of triangles in \mathbb{R}^2 and tetrahedra in \mathbb{R}^3 . Let us associate with K_h a mesh function $h_K = \text{diam}(K)$, $\forall x \in K$, representing the diameter of the element K . For the time discretization, let $J_k = \{J\}$ be a partition of the time interval $I = (0, T]$ into time intervals $J = (t_{k-1}, t_k]$ of uniform length $\tau = t_k - t_{k-1}$.

We define the following L_2 inner products and norm

$$(p, q) = \int_{\Omega} pq \, dx, \quad ((p, q)) = \int_{\Omega} \int_0^T pq \, dt \, dx, \quad \|p\|^2 = ((p, p)).$$

We introduce the finite element trial space W_h^v defined by :

$$W_h^v := \{v \in W_1^v \cup W_2^v : v|_{K \times J} \in P_1(K) \times P_1(J), \forall K \in K_h, \forall J \in J_k\},$$

where

$$W_1^v := \{v \in H^1(\Omega \times J) : v(\cdot, 0) = 0, \partial_n v|_{\Gamma_1} = v_1, \partial_n v|_{\Gamma_2} = Dv, \partial_n v|_{\Gamma_3} = 0\},$$

$$W_2^v := \{v \in H^1(\Omega \times J) : v(\cdot, 0) = 0, \partial_n v|_{\Gamma_1} = \partial_n v|_{\Gamma_2} = Dv, \partial_n v|_{\Gamma_3} = 0\}.$$

Here $P_1(K)$ and $P_1(J)$ are the set of linear functions on K and J , respectively.

Furthermore, the finite element space W_h^λ for the costate λ , is defined by:

$$W_h^\lambda := \{\lambda \in W_1^\lambda \cup W_2^\lambda : \lambda|_{K \times J} \in P_1(K) \times P_1(J), \forall K \in K_h, \forall J \in J_k\},$$

where

$$W_1^\lambda := \{\lambda \in H^1(\Omega \times J) : \lambda(\cdot, T) = 0, \partial_n \lambda|_{\Gamma_1} = \partial_n \lambda|_{\Gamma_3} = 0, \partial_n \lambda|_{\Gamma_2} = D\lambda\},$$

$$W_2^\lambda := \{\lambda \in H^1(\Omega \times J) : \lambda(\cdot, T) = 0, \partial_n \lambda|_{\Gamma_1} = \partial_n \lambda|_{\Gamma_2} = D\lambda, \partial_n \lambda|_{\Gamma_3} = 0\}.$$

The finite element method for (3)-(4) now reads: Find $E_h \in W_h^v$ such that $\forall \bar{\lambda} \in W_h^\lambda$,

$$\begin{aligned} & - ((\epsilon DE_h, D\bar{\lambda})) + ((\nabla E_h, \nabla \bar{\lambda})) \\ & - ((DE_h, \bar{\lambda}))_{(t_1, T] \times \Gamma_1} - ((DE_h, \bar{\lambda}))_{(0, T] \times \Gamma_2} = ((v_1, \bar{\lambda}))_{(0, t_1] \times \Gamma_1}. \end{aligned} \tag{5}$$

Here, the initial condition $DE(0) = 0$ is imposed in weak form through the variational formulation.

Expanding E and λ in terms of the standard continuous piecewise linear functions $\varphi_i(x)$ in space and $\psi_i(t)$ in time, and substituting this into (5), we obtain an explicit scheme for solving (5), see for example [3] where a similar system is obtained for an acoustic wave equation with homogenous boundary conditions.

4 The inverse problem

We formulate the inverse problem for (3) and (4) as follows: given the function $\partial_n E = v_1$ on $\Gamma_1 \times (0, t_1]$, determine the coefficient $\epsilon(x)$ for $x \in \Omega$, which minimizes the quantity

$$J(E, \epsilon) = \frac{1}{2} \int_0^T \int_{\Omega} (E - \tilde{E})^2 \delta_{obs} dxdt + \frac{1}{2} \gamma \int_{\Omega} (\epsilon - \epsilon_0)^2 dx. \quad (6)$$

Here \tilde{E} is the data observed at a finite set of points x_{obs} , E satisfies (3) and (4) and thus depends on ϵ . Moreover, $\delta_{obs} = \sum \delta(x - x_{obs})$ is a sum of delta-functions corresponding to the observation points, γ is a regularization parameter, and ϵ_0 is the initial guess value for the parameter we want to reconstruct.

To solve this minimization problem, we introduce the Lagrangian

$$L(u) = J(E, \epsilon) - ((\epsilon DE, D\lambda)) + ((\nabla E, \nabla \lambda)) - ((DE, \lambda))_{(t_1, T] \times \Gamma_1} - ((DE, \lambda))_{(0, T] \times \Gamma_2} - ((v_1, \lambda))_{(0, t_1] \times \Gamma_1}, \quad (7)$$

where $u = (E, \lambda, \epsilon)$, and search for a stationary point with respect to u , satisfying for all $\bar{u} = (\bar{E}, \bar{\lambda}, \bar{\epsilon})$

$$L'(u; \bar{u}) = 0, \quad (8)$$

where L' is the gradient of L . Equation (8) expresses that for all \bar{u} ,

$$\begin{aligned} \frac{\partial L(u)}{\partial \lambda}(\bar{\lambda}) &= -((\epsilon D\bar{\lambda}, DE)) + ((\nabla E, \nabla \bar{\lambda})) - ((DE, \bar{\lambda}))_{(t_1, T] \times \Gamma_1} \\ &\quad - ((DE, \bar{\lambda}))_{(0, T] \times \Gamma_2} - ((2v_1, \bar{\lambda}))_{(0, t_1] \times \Gamma_1} = 0, \\ \frac{\partial L(u)}{\partial E}(\bar{E}) &= ((E - \tilde{E}, \bar{E}))_{\delta_{obs}} - ((\epsilon D\lambda, D\bar{E})) + ((\nabla \lambda, \nabla \bar{E})) \\ &\quad + ((D\lambda, \bar{E}))_{[0, T] \times \Gamma_1} + ((D\lambda, \bar{E}))_{[0, T] \times \Gamma_2} = 0, \\ \frac{\partial L(u)}{\partial \epsilon}(\bar{\epsilon}) &= -((D\lambda DE, \bar{\epsilon})) + \gamma(\epsilon - \epsilon_0, \bar{\epsilon}) = 0. \end{aligned} \quad (9)$$

The first equation in (9) is a weak form of the state equation (3) and (4), the second equation is a weak form of the adjoint state equation,

$$\begin{aligned} \epsilon \frac{\partial^2 \lambda}{\partial t^2} - \nabla \cdot (\nabla \lambda) &= -(E - \tilde{E})\delta_{obs}, \quad x \in \Omega, \quad 0 \leq t < T, \\ \partial_n \lambda &= 0 \text{ on } \Gamma_1 \times [0, t_1], \\ \partial_n \lambda &= D\lambda \text{ on } \Gamma_1 \times [0, T], \\ \partial_n \lambda &= D\lambda \text{ on } \Gamma_2 \times [0, T], \\ \partial_n \lambda &= 0 \text{ on } \Gamma_3 \times [0, T], \\ \lambda(\cdot, T) &= D\lambda(\cdot, T) = 0 \text{ in } \Omega, \end{aligned} \quad (10)$$

and the last equation expresses stationarity with respect to the parameter ϵ .

5 A finite element method for inverse problem

To formulate a finite element method for (8) we introduce the finite element space V_h of piecewise constants for the coefficient $\epsilon(x)$, defined by :

$$V_h := \{v \in L_2(\Omega) : v \in P_0(K), \forall K \in K_h\}.$$

Recalling the definitions of W_h^v and W_h^λ , related to the state E and the costate λ , and defining $U_h = W_h^v \times W_h^\lambda \times V_h$, we formulate the finite element method for (8) as: Find $u_h \in U_h$, such that

$$L'(u_h; \bar{u}) = 0, \quad \forall \bar{u} \in U_h. \quad (11)$$

6 An a posteriori error estimate for the Lagrangian

Theorem 6.1. *Let $L(u) = L(E, \lambda, \epsilon)$ be the Lagrangian as defined in (7), and let $L(u_h) = L(E_h, \lambda_h, \epsilon_h)$ be the approximation of $L(u)$. Then the following representation holds for the error $e = L(u) - L(u_h)$:*

$$\begin{aligned} |e| \leq & ((R_{E_1}, \sigma_\lambda))_{(0,t_1] \times \Gamma_1} + ((R_{E_2}, \sigma_\lambda)) + ((R_{E_3}, \sigma_\lambda)) \\ & + ((R_{E_4}, \sigma_\lambda))_{(t_1, T] \times \Gamma_1} + ((R_{E_5}, \sigma_\lambda))_{(0, T] \times \Gamma_2} \\ & + ((R_{\lambda_1}, \sigma_E))_{\delta_{obs}} + ((R_{\lambda_2}, \sigma_E)) + ((R_{\lambda_3}, \sigma_E)) \\ & + ((R_{\lambda_4}, \sigma_E))_{(0, T] \times \Gamma_1} + ((R_{\lambda_5}, \sigma_E))_{(0, T] \times \Gamma_2} \\ & + ((R_{\epsilon_1}, \sigma_\epsilon)) + (R_{\epsilon_2}, \sigma_\epsilon), \end{aligned} \quad (12)$$

where the residuals are defined by

$$\begin{aligned} R_{E_1} &= 2|v_1|, \quad R_{E_2} = \max_{S \subset \partial K} h_K^{-1} |[\partial_s E_h]|, \\ R_{E_3} &= \epsilon_h \tau^{-1} |[\partial_t E_h]|, \quad R_{E_4} = R_{E_5} = |DE_h|, \\ R_{\lambda_1} &= |E_h - \tilde{E}|, \quad R_{\lambda_2} = \max_{S \subset \partial K} h_K^{-1} |[\partial_s \lambda_h]|, \\ R_{\lambda_3} &= \epsilon_h \tau^{-1} |[\partial_t \lambda_h]|, \quad R_{\lambda_4} = R_{\lambda_5} = |D\lambda_h|, \\ R_{\epsilon_1} &= |D\lambda_h| \cdot |DE_h|, \quad R_{\epsilon_2} = \gamma |\epsilon_h - \epsilon_0|, \end{aligned}$$

and the interpolation errors are

$$\begin{aligned} \sigma_\lambda &= C\tau | [D\lambda_h] | + Ch_K | [\partial_n \lambda_h] |, \\ \sigma_E &= C\tau | [DE_h] | + Ch_K | [\partial_n E_h] |, \\ \sigma_\epsilon &= C | [\epsilon_h] |, \end{aligned}$$

Here, $[v]$ denotes the maximum of the modulus of a jump of v across the face of an element K (or the boundary node of a time interval J), $\partial_s v$ denotes the normal derivative of v across a side of K , $\partial_n v$ denotes the derivative of v in the outward normal of an element K , $[\partial_t v]$ is the maximum modulus of the jump of the time derivative of v across a boundary node of J , C is interpolation constants of moderate size.

Proof. Throughout the proof, let C denote different constants of a moderate size.

As in [1], we use the fundamental theorem of calculus to write

$$\begin{aligned} e &= L(v) - L(v_h) \\ &= \int_0^1 \frac{d}{ds} L(v_h + s(v - v_h)) ds \\ &= \int_0^1 L'(v_h + s(v - v_h); v - v_h) ds \\ &= L'(v_h; v - v_h) + R, \end{aligned}$$

where R denotes a second order term. For full details of the arguments we refer to [1] and [7].

Neglecting the term R , and using the Galerkin orthogonality (11) with the splitting

$$v - v_h = (v - v_h^I) + (v_h^I - v_h), \quad (13)$$

where v_h^I denotes an interpolant of v , leads to the following error representation:

$$e \approx L'(v_h; v - v_h^I) = I_1 + I_2 + I_3. \quad (14)$$

Here

$$\begin{aligned} I_1 &= - \left((\epsilon_h D E_h, D(\lambda - \lambda_h^I)) \right) + \left((\nabla E_h, \nabla(\lambda - \lambda_h^I)) \right) - \left((2v_1, \lambda - \lambda_h^I) \right)_{(0,t_1] \times \Gamma_1} \\ &\quad - \left((D E_h, \lambda - \lambda_h^I) \right)_{(t_1, T] \times \Gamma_1} - \left((D E_h, \lambda - \lambda_h^I) \right)_{(0, T] \times \Gamma_2}, \\ I_2 &= \left((E_h - \tilde{E}, E - E_h^I) \right)_{\delta_{obs}} - \left((\epsilon_h D \lambda_h, D(E - E_h^I)) \right) + \left((\nabla \lambda_h, \nabla(E - E_h^I)) \right) \\ &\quad + \left((D \lambda_h, E - E_h^I) \right)_{(0, T] \times \Gamma_1} + \left((D \lambda_h, E - E_h^I) \right)_{(0, T] \times \Gamma_2}, \\ I_3 &= - \left((D \lambda_h D E_h, \epsilon - \epsilon_h^I) \right) + \gamma(\epsilon_h - \epsilon_0, \epsilon - \epsilon_h^I), \end{aligned}$$

To estimate I_1 , we integrate by parts in the first and second terms to obtain:

$$\begin{aligned} |I_1| &= \left| \left((\epsilon_h D^2 E_h, \lambda - \lambda_h^I) \right) - \left((\Delta E_h, \lambda - \lambda_h^I) \right) \right. \\ &\quad - \left((2v_1, \lambda - \lambda_h^I) \right)_{(0,t_1] \times \Gamma_1} - \left((D E_h, \lambda - \lambda_h^I) \right)_{(t_1, T] \times \Gamma_1} \\ &\quad - \left((D E_h, \lambda - \lambda_h^I) \right)_{(0, T] \times \Gamma_2} \\ &\quad - \sum_k \int_{\Omega} \epsilon_h [D E_h(t_k)] (\lambda - \lambda_h^I)(t_k) \, dx \\ &\quad \left. + \sum_K \int_0^T \int_{\partial K} \partial_n E_h (\lambda - \lambda_h^I) \, ds dt \right|, \end{aligned} \quad (15)$$

Here, $[D E_h(t_k)]$ denote the jump of the derivative of E_h at time t_k (see Figure 2), and $\partial_n E_h$ denote the derivative of E_h in the outward normal direction n of the boundary ∂K of element K .

Since E_h is a piecewise linear function, the terms $D^2 E_h$ and ΔE_h in (15) disappear, and we get:

$$\begin{aligned} |I_1| &= \left| - \left((2v_1, \lambda - \lambda_h^I) \right)_{(0,t_1] \times \Gamma_1} - \left((D E_h, \lambda - \lambda_h^I) \right)_{(t_1, T] \times \Gamma_1} \right. \\ &\quad - \left((D E_h, \lambda - \lambda_h^I) \right)_{(0, T] \times \Gamma_2} \\ &\quad - \sum_k \int_{\Omega} \epsilon_h [D E_h(t_k)] (\lambda - \lambda_h^I)(t_k) \, dx \\ &\quad \left. + \sum_K \int_0^T \int_{\partial K} \partial_n E_h (\lambda - \lambda_h^I) \, ds dt \right|. \end{aligned} \quad (16)$$

In the last term of equation (16) we sum over the element boundaries, where each interior side $S \in S_h$ occurs twice, see Figure 1. Denoting by $\partial_{n^\pm} E_h$ the derivative of E_h in the outward normal direction n^\pm to element K^\pm , and by $\partial_s E_h$ the derivative of a function E_h in one of the normal directions, n^- and n^+ , of each side S , we can write

$$\sum_K \int_{\partial K} \partial_n E_h (\lambda - \lambda_h^I) \, ds = \sum_S \int_S [\partial_s E_h] (\lambda - \lambda_h^I) \, ds, \quad (17)$$

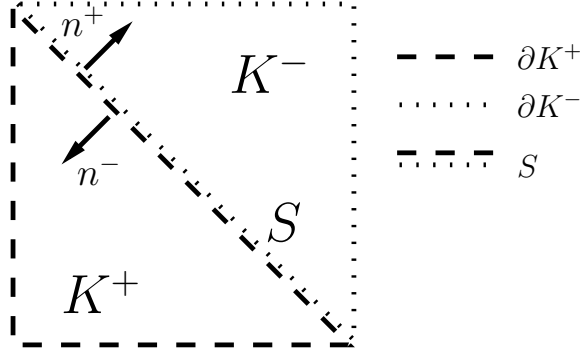


Figure 1: Two neighbouring elements K^+ and K^- , their boundaries, ∂K^+ and ∂K^- , and the interior side S .

where the jump $[\partial_s E_h]$ is defined as

$$[\partial_s E_h] = \max_{S \in \partial K} \{\partial_{n^+} E_h, \partial_{n^-} E_h\}.$$

We distribute each jump equally to the two sharing elements and return to a sum of the element edges ∂K :

$$\sum_S \int_S [\partial_s E_h] (\lambda - \lambda_h^I) ds = \sum_K \frac{1}{2} \int_{\partial K} [\partial_s E_h] (\lambda - \lambda_h^I) ds. \quad (18)$$

We multiply and divide by h_K , formally set $dx = h_K ds$ and replace the integrals over the element boundaries ∂K by integrals over the elements K , to get:

$$\begin{aligned} & \left| \sum_K \frac{1}{2} h_K^{-1} \int_{\partial K} [\partial_s E_h] (\lambda - \lambda_h^I) h_K ds \right| \\ & \leq C \int_{\Omega} \max_{S \subset \partial K} h_K^{-1} |[\partial_s E_h]| |\lambda - \lambda_h^I| dx, \end{aligned} \quad (19)$$

where $[\partial_s E_h]|_K = \max_{S \subset \partial K} |[\partial_s E_h]|_S$.

In a similar way we can estimate the jump in time in (16) by multiplying and dividing by τ :

$$\begin{aligned} & \left| \sum_k \int_{\Omega} \epsilon_h [DE_h(t_k)] (\lambda - \lambda_h^I)(t_k) dx \right| \\ & \leq \sum_k \int_{\Omega} \epsilon_h \tau^{-1} | [DE_h(t_k)] | |(\lambda - \lambda_h^I)(t_k)| \tau dx \\ & \leq C \sum_k \int_{J_k} \int_{\Omega} \epsilon_h \tau^{-1} | [\partial_{t_k} E_h] | |\lambda - \lambda_h^I| dx dt \\ & = C ((\epsilon_h \tau^{-1} | [\partial_t E_h] |, |(\lambda - \lambda_h^I)|)). \end{aligned} \quad (20)$$

Here, we have defined $[\partial_{t_k} E_h]$ as the greatest of the two jumps on the interval $(t_k, t_{k+1}]$:

$$[\partial_{t_k} E_h] = \max_k ([DE_h(t_k)], [DE_h(t_{k+1})]),$$

$$[\partial_t E_h] = [\partial_{t_k} E_h] \text{ on } J_k.$$

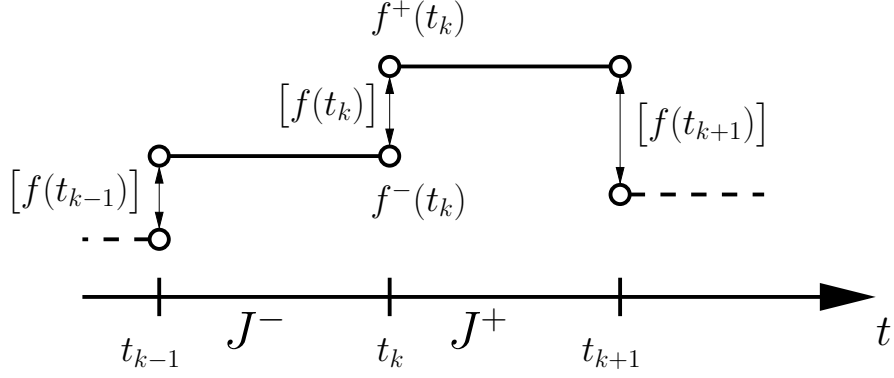


Figure 2: The jump of a function f on the time mesh.

where $[DE_h(t_k)] = DE_h^+(t_k) - DE_h^-(t_k)$. The time jumps are illustrated in Figure 2.

We substitute the expressions (19) and (20) in (16), to get:

$$\begin{aligned}
|I_1| \leq & ((2|v_1|, |\lambda - \lambda_h^I|))_{(0,t_1] \times \Gamma_1} - ((|DE_h|, |\lambda - \lambda_h^I|))_{(t_1, T] \times \Gamma_1} \\
& - ((|DE_h|, |\lambda - \lambda_h^I|))_{(0, T] \times \Gamma_2} \\
& + C((\max_{S \subset \partial K} h_K^{-1} |[\partial_s E_h]|, |\lambda - \lambda_h^I|)) \\
& + C((\epsilon_h \tau^{-1} |[\partial_t E_h]|, |\lambda - \lambda_h^I|)).
\end{aligned}$$

Next, we use the following standard interpolation estimate

$$|\lambda - \lambda_h^I| \leq C(\tau^2 |D^2 \lambda| + h_K^2 |D_x^2 \lambda|), \quad (21)$$

where we approximate the second derivative in time as

$$D^2 \lambda = \frac{\partial^2 \lambda}{\partial t^2} = \frac{\partial(D\lambda)}{\partial t} \approx \frac{(D\lambda)^+ - (D\lambda)^-}{\tau} = \frac{[D\lambda_h]}{\tau}.$$

Here $(\cdot)^+$ and $(\cdot)^-$ represents values on two neighbouring intervals J^+ and J^- , see Figure 2. In the same way we approximate the second derivative in space:

$$D_x^2 \lambda \approx \frac{[\partial_n \lambda_h]}{h}.$$

Substituting both expressions above in (21), we obtain

$$|\lambda - \lambda_h^I| \leq C(\tau |[D\lambda_h]| + h_K |[\partial_n \lambda_h]|) \quad (22)$$

and the estimate for I_1 reduces to

$$\begin{aligned}
|I_1| \leq & C((2|v_1|, \tau |[D\lambda_h]| + h_K |[\partial_n \lambda_h]|))_{(0,t_1] \times \Gamma_1} \\
& - C((|DE_h|, \tau |[D\lambda_h]| + h_K |[\partial_n \lambda_h]|))_{(t_1, T] \times \Gamma_1} \\
& - C((|DE_h|, \tau |[D\lambda_h]| + h_K |[\partial_n \lambda_h]|))_{(0, T] \times \Gamma_2} \\
& + C((\max_{S \subset \partial K} h_k^{-1} |[\partial_s E_h]|, \tau |[D\lambda_h]| + h_K |[\partial_n \lambda_h]|)) \\
& + C((\epsilon_h \tau^{-1} |[\partial_t E_h]|, \tau |[D\lambda_h]| + h_K |[\partial_n \lambda_h]|)).
\end{aligned}$$

We estimate I_2 similarly as I_1 . First, we integrate by parts to obtain

$$\begin{aligned}
|I_2| \leq & |((E_h - \tilde{E}, E - E_h^I))_{\delta_{obs}} + ((\epsilon_h D^2 \lambda_h, E - E_h^I)) \\
& - ((\Delta \lambda_h, E - E_h^I)) + ((D \lambda_h, E - E_h^I))_{(0,T] \times \Gamma_1} \\
& + ((D \lambda_h, E - E_h^I))_{(0,T] \times \Gamma_2} | \\
& + C \left(\left(\max_{S \subset \partial K} h_K^{-1} |[\partial_s \lambda_h]|, |E - E_h^I| \right) \right) \\
& + C \left((\epsilon_h \tau^{-1} |[\partial_t \lambda_h]|, |E - E_h^I| \right).
\end{aligned}$$

Since λ_h is piecewise linear, the terms with $\Delta \lambda_h$ and $D^2 \lambda_h$ will disappear:

$$\begin{aligned}
|I_2| \leq & ((|E_h - \tilde{E}|, |E - E_h^I|))_{\delta_{obs}} \\
& + ((|D \lambda_h|, |E - E_h^I|))_{(0,T] \times \Gamma_1} \\
& + ((|D \lambda_h|, |E - E_h^I|))_{(0,T] \times \Gamma_2} \\
& + C \left(\left(\max_{S \subset \partial K} h_K^{-1} |[\partial_s \lambda_h]|, |E - E_h^I| \right) \right) \\
& + C \left((\epsilon_h \tau^{-1} |[\partial_t \lambda_h]|, |E - E_h^I|) \right).
\end{aligned}$$

Next, we use the same kind of interpolation estimate for $|E - E_h^I|$ as we found for $|\lambda - \lambda_h^I|$ in equation (22), to get:

$$\begin{aligned}
|I_2| \leq & C \left((|E_h - \tilde{E}|, \tau | [DE_h] | + h_K | [\partial_n E_h] |) \right)_{\delta_{obs}} \\
& + C \left((|D \lambda_h|, \tau | [DE_h] | + h_K | [\partial_n E_h] |) \right)_{(0,T] \times \Gamma_1} \\
& + C \left((|D \lambda_h|, \tau | [DE_h] | + h_K | [\partial_n E_h] |) \right)_{(0,T] \times \Gamma_2} \\
& + C \left(\left(\max_{S \subset \partial K} h_K^{-1} |[\partial_s \lambda_h]|, \tau | [DE_h] | + h_K | [\partial_n E_h] | \right) \right) \\
& + C \left((\epsilon_h \tau^{-1} |[\partial_t \lambda_h]|, \tau | [DE_h] | + h_K | [\partial_n E_h] |) \right).
\end{aligned}$$

To estimate I_3 we use the following approximation estimate for $\epsilon - \epsilon_h^I$:

$$|\epsilon - \epsilon_h^I| \leq Ch_K D_x \epsilon \leq Ch_K \left| \frac{[\epsilon_h]}{h_K} \right| \leq C |[\epsilon_h]|,$$

and we end up with

$$|I_3| \leq ((|D \lambda_h| |DE_h|, |[\epsilon_h]|)) + \gamma (|\epsilon_h - \epsilon_0|, |[\epsilon_h]|),$$

which completes the proof. \square

7 A posteriori error estimation for parameter identification

Following [4] we present a more general a posteriori estimate for the error in the reconstructed parameter. We first note that

$$\begin{aligned}
L'(u; \tilde{u}) - L'(u_h; \tilde{u}) &= \int_0^1 \frac{d}{ds} L'(us + (1-s)u_h; \tilde{u}) ds \\
&= \int_0^1 L''(us + (1-s)u_h; u - u_h, \tilde{u}) ds \\
&= L''(u_h; u - u_h, \tilde{u}) + R,
\end{aligned}$$

where R is a second order remainder and $L''(u_h; \cdot, \cdot)$ is the Hessian of the Lagrangian. Since $L'(u; \tilde{u}) = 0$, we get

$$-L''(u_h; u - u_h, \tilde{u}) = L'(u_h; \tilde{u}) + R.$$

Next, we can use the Galerkin orthogonality (11) with the splitting $\tilde{u} - \tilde{u}_h = (\tilde{u} - \tilde{u}_h^I) + (\tilde{u}_h^I - \tilde{u}_h)$, where $\tilde{u}_h^I \in U_h$ denotes an interpolant of \tilde{u} , to get the following equation

$$-L''(u_h; u - u_h, \tilde{u}) = L'(u_h; \tilde{u} - \tilde{u}_h^I) + R. \quad (23)$$

In our case the dual problem is defined as

$$-L''(u_h; u - u_h, \tilde{u}) = (\psi, u - u_h), \quad (24)$$

where ψ is a given data. Neglecting the term R in (23), and comparing (23) with (24), we get

$$(\psi, u - u_h) \approx L'(u_h; \tilde{u} - \tilde{u}_h^I). \quad (25)$$

From this estimate we observe that the form of the error for a parameter identification is similar to the error in the Lagrangian, if the weight u is replaced by \tilde{u} .

We can choose $u - u_h = \bar{u}$ in (24) and the dual problem can be written as

$$-L''(u_h; \bar{u}, \tilde{u}) = (\psi, \bar{u}). \quad (26)$$

We conclude that for an appropriate choice of the data, ψ , in the dual problem, we can solve (26) approximately for \tilde{u} and thus get values of the error for \bar{u} .

8 The Hessian of the Lagrangian

In Section 7 we presented an a posteriori error estimate for identification of the parameter. In this section we derive an approximation of the strong form of the dual problem (26), which can be used to calculate the weights for the problem (3)-(4).

The Hessian of the Lagrangian (7) takes the following form

$$L''(u; \bar{u}, \tilde{u}) = L''_E(u; \bar{u}, \tilde{E}) + L''_\lambda(u; \bar{u}, \tilde{\lambda}) + L''_\epsilon(u; \bar{u}, \tilde{\epsilon}), \quad (27)$$

where

$$\begin{aligned} L''_E(u; \bar{u}, \tilde{E}) &= -((\epsilon D\bar{\lambda}, D\tilde{E})) + ((\nabla\tilde{E}, \nabla\bar{\lambda})) + ((\tilde{E}, \bar{E}))_{\delta_{obs}} - ((D\tilde{E}D\bar{\lambda}, \bar{\epsilon})) \\ &\quad - ((D\tilde{E}, \bar{\lambda}))_{[0, T] \times \Gamma_1} - ((D\tilde{E}, \bar{\lambda}))_{[0, T] \times \Gamma_2}, \\ L''_\lambda(u; \bar{u}, \tilde{\lambda}) &= -((\epsilon D\tilde{E}, D\tilde{\lambda})) + ((\nabla\tilde{\lambda}, \nabla\tilde{E})) - ((v_1, \tilde{\lambda}))_{(0, t_1] \times \Gamma_1} - ((DED\tilde{\lambda}, \bar{\epsilon})) \\ &\quad - ((D\tilde{\lambda}, \bar{E}))_{(t_1, T] \times \Gamma_1} - ((D\tilde{\lambda}, \bar{E}))_{(0, T] \times \Gamma_2}, \\ L''_\epsilon(u; \bar{u}, \tilde{\epsilon}) &= -((DED\bar{\lambda}, \tilde{\epsilon})) - ((D\lambda D\tilde{E}, \tilde{\epsilon})) + \gamma(\bar{\epsilon}, \tilde{\epsilon}). \end{aligned}$$

Here we have used the boundary conditions $\partial_n \lambda = D\lambda$, $\partial_n \tilde{\lambda} = D\tilde{\lambda}$, $\partial_n \bar{\lambda} = D\bar{\lambda}$ on $\Gamma_1 \cup \Gamma_2 \times [0, T)$, and $\partial_n E = \partial_n \bar{E} = \partial_n \tilde{E} = v_1|_{(0, t_1] \times \Gamma_1}$, $\partial_n E = DE$, $\partial_n \bar{E} = D\bar{E}$, $\partial_n \tilde{E} = D\tilde{E}$ on $\Gamma_1 \times (t_1, T]$ and $\Gamma_2 \times (0, T]$, respectively.

Then the dual problem (26) takes the following strong form

$$\begin{aligned} \epsilon \frac{\partial^2 \tilde{\lambda}}{\partial t^2} - \nabla \cdot (\nabla \tilde{\lambda}) + \tilde{E}_{\delta_{obs}} + \tilde{\epsilon} \frac{\partial^2 \lambda}{\partial t^2} - D\tilde{\lambda}_{(t_1, T) \times \Gamma_1} - D\tilde{\lambda}_{(0, T) \times \Gamma_2} &= \psi_1, \\ \epsilon \frac{\partial^2 \tilde{E}}{\partial t^2} - \nabla \cdot \left(\frac{1}{\epsilon} \nabla \tilde{E} \right) + \tilde{\epsilon} \frac{\partial^2 E}{\partial t^2} - v_1|_{(0, t_1] \times \Gamma_1} - D\tilde{E}_{(t_1, T) \times \Gamma_1} - D\tilde{E}_{(0, T) \times \Gamma_2} &= \psi_2, \\ - \int_0^T D\lambda D\tilde{E} dt - \int_0^T D\tilde{\lambda} DE dt + \gamma_1 \tilde{\epsilon} &= \psi_3, \end{aligned} \quad (28)$$

with initial and boundary conditions. Our goal is to solve the system (28) with an already known approximation to the final solution u , computed using the adaptive Algorithm 2 in Section 9, and find $\tilde{u} = (\tilde{E}, \tilde{\lambda}, \tilde{\epsilon})$. We assume that the solution of the adjoint problem, λ , will be small after the final optimization iteration, and we can neglect all terms involving λ to get the following approximated problem

$$\begin{aligned} \epsilon \frac{\partial^2 \tilde{\lambda}}{\partial t^2} - \nabla \cdot (\nabla \tilde{\lambda}) + \tilde{E}_{\delta_{obs}} - D\tilde{\lambda}_{(t_1, T) \times \Gamma_1} - D\tilde{\lambda}_{(0, T) \times \Gamma_2} &= \psi_1, \\ \epsilon \frac{\partial^2 \tilde{E}}{\partial t^2} - \nabla \cdot (\nabla \tilde{E}) + \tilde{\epsilon} \frac{\partial^2 E}{\partial t^2} - v_1|_{(0, t_1] \times \Gamma_1} - D\tilde{E}_{(t_1, T) \times \Gamma_1} - D\tilde{E}_{(0, T) \times \Gamma_2} &= \psi_2, \\ - \int_0^T D\tilde{\lambda} D E dt + \gamma \tilde{\epsilon} &= \psi_3. \end{aligned} \quad (29)$$

As already mentioned in [4], the stability properties of this system is an open problem.

9 Adaptive algorithms for the inverse problem

In this section we present two different adaptive algorithms for solution of the inverse problem presented in Section 4. In Algorithm 1, the refinement is based on computations of the residuals for the parameter, since they already give a good indication where to refine the mesh. The interpolation errors, and thus the exact value of the computational error in the reconstructed parameter, can be obtained by computing the Hessian of the Lagrangian using equation (29) as shown in Algorithm 2.

As we see from (12), the error in the Lagrangian consists of integrals in space and time of the different residuals multiplied by the interpolation errors. Thus, to estimate the error in the Lagrangian we need to compute the approximated values of $(E_h, \lambda_h, \epsilon_h)$ together with residuals and interpolation errors. Since we want to control the error in the reconstructed parameter, ϵ_h , we limit the computations to R_{ϵ_1} and R_{ϵ_2} , and neglect to compute the other residuals in the a posteriori estimate (12). The a posteriori error in step 5 of Algorithm 1 is thus calculated as

$$e(x) \approx \int_0^T R_{\alpha_1}(x, t) dt + R_{\alpha_2}(x). \quad (30)$$

9.1 Algorithm 1

0. Choose an initial mesh K_h and an initial time partition J_0 of the time interval $(0, T]$. Start with an initial guess ϵ^0 , and compute the sequence of ϵ^n in the following steps:
1. Compute the solution E^n of the forward problem (3)-(4) on K_h and J_k , with $\epsilon(x) = \epsilon^{(n)}$.
2. Compute the solution λ^n of the adjoint problem (10) on K_h and J_k .
3. Update the parameter ϵ on K_h and J_k using the quasi-Newton method

$$\epsilon^{n+1} = \epsilon^n + \alpha^n H^n g^n,$$

where H^n is an approximate Hessian, computed using the usual BFGS update formula for the Hessian, see [8]. Furthermore, g^n is the gradient of the Lagrangian (7)

with respect to the parameter ϵ ,

$$g^n = - \int_0^T D\lambda^n DE^n dt + \gamma(\epsilon^n - \epsilon_0), \quad (31)$$

where α is the step length in the parameter upgrade computed using an one-dimensional search algorithm [9].

4. Stop computing ϵ if the gradient $g^n < \eta$; if not set $n = n + 1$ and go to step 1. Here, η is the tolerance in the quasi-Newton update.
5. Compute the residuals, $R_{\epsilon_1}, R_{\epsilon_2}$ and refine the mesh in all points where

$$\int_0^T R_{\alpha_1}(x, t) dt + R_{\alpha_2}(x) < tol \quad (32)$$

is violated. Here tol is a tolerance chosen by the user.

6. Construct a new mesh K_h and a new time partition J_k . Return to step 1 and perform all the steps of the optimization algorithm on the new mesh.

9.2 Algorithm 2

0. Choose an initial mesh K_h and an initial time partition J_0 of the time interval $(0, T]$. Start with an initial guess ϵ^0 , and compute a sequence of ϵ^n in the following steps:
 1. Compute the solution E^n of the forward problem (3)-(4) on K_h and J_k with $\epsilon(x) = \epsilon^{(n)}$.
 2. Compute the solution λ^n of the adjoint problem (10) on K_h and J_k .
 3. Update the parameter ϵ on K_h and J_k using the quasi-Newton method

$$\epsilon^{n+1} = \epsilon^n + \alpha^n H^n g^n,$$

where H^n is an approximate Hessian, and g^n is the gradient of the Lagrangian (7) with respect to the parameter ϵ , as in equation (31).

4. Stop if the gradient $g^n < \eta$; if not, set $n = n + 1$ and go to step 1. Here, η is the tolerance in the quasi-Newton update.
5. Compute the residuals, R_{ϵ_1} and R_{ϵ_2} , in (25).
6. Compute the weight $\sigma_{\tilde{\epsilon}}$ in the a posteriori error estimate, (25), by solving equation (29), using the following iterative procedure:

- 6.1. From the last equation in (29), update $\tilde{\epsilon}$ as

$$\tilde{\epsilon}^{m+1} = \tilde{\epsilon}^m + \tilde{\alpha}(\psi_3 + \int_0^T D\tilde{\lambda}^m DE_h dt - \gamma\tilde{\epsilon}^m), \quad (33)$$

where $\tilde{\alpha} > 0$ is the step length.

- 6.2. Solve the second equation in (29) and find \tilde{E} .
- 6.3. Solve the first equation in (29) and find $\tilde{\lambda}$.

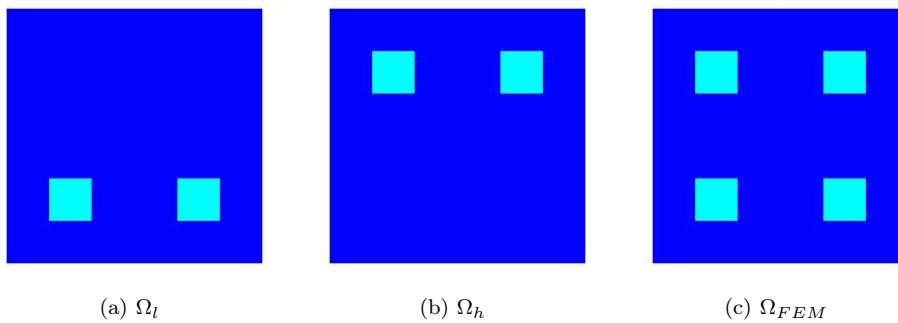


Figure 3: We show the square lattice of a crystal where the material to be reconstructed is a square lattice of columns.

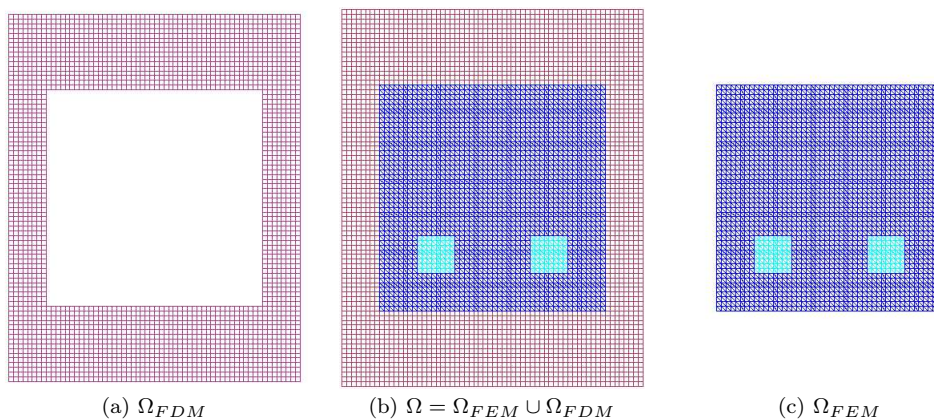


Figure 4: The hybrid mesh (b) is a combinations of a structured mesh (a), where FDM is applied, and a mesh (c), where we use FEM, with a thin overlapping of structured elements.

6.4. Compute (33) until $\|\tilde{\epsilon}^{m+1} - \tilde{\epsilon}^m\| < eps$, where $eps > 0$ is a tolerance, otherwise; choose $\tilde{\epsilon}^m = \tilde{\epsilon}^{m+1}$ and return to 6.1.

7. Compute the value of the *error* in the reconstructed parameter ϵ using (25) as

$$error = ((R_{\epsilon_1}, \sigma_{\tilde{\epsilon}})) + (R_{\epsilon_2}, \sigma_{\tilde{\epsilon}}),$$

where $\sigma_{\tilde{\epsilon}} = C|[\tilde{\epsilon}_h]|$, on the mesh K_h .

8. Refine all elements where $|error| > tol$. Here tol is a tolerance chosen by the user.

9. Construct a new mesh K_h and a new time partition J_k . Return to step 1 and perform all steps of the optimization algorithm on the new mesh.

10 Numerical Results

In this section we present several numerical examples to show the performance of the adaptive hybrid method and the usefulness of the a posteriori error estimate (12).

The computational domain, $\Omega = \Omega_{FEM} \cup \Omega_{FDM}$, is set as $\Omega = [-4.0, 4.0] \times [-5.0, 5.0]$. Next, Ω is split into a finite element domain $\Omega_{FEM} = [-3.0, 3.0] \times [-3.0, 3.0]$ with an unstructured mesh and a surrounding domain Ω_{FDM} with a structured mesh, see Fig. 4.

opt.it.	625 nodes	809 nodes	1263 nodes	2225 nodes
1	0.0118349	0.0108764	0.0108764	0.010476
2	0.0095824	0.00987447	0.00965067	0.00954041
3	0.00822312	0.00709372	0.00558728	0.00769998
4	0.00748565	0.00318215	0.00273809	0.00313069
5	0.00619674	0.00291434		
6	0.00528474			
7	0.00471419			
8	0.00354939			

Table 1: $\|E - E_{obs}\|_{L^2}$ on the four adaptively refined meshes in the reconstruction of the lower squares. The number of stored corrections in the quasi-Newton method is $m = 15$. The computations was performed with noise level $\sigma = 0$ and regularization parameter $\gamma = 0.1$.

Between Ω_{FEM} and Ω_{FDM} there is a thin overlap. The space mesh consists of triangles in Ω_{FEM} , and squares in Ω_{FDM} . In Ω_{FDM} and the overlapping region, the mesh size is $h = 0.25$ and $h = 0.125$, in Example 1 and Example 2, respectively. We apply the hybrid finite element/difference method presented in [5] where finite elements are used in Ω_{FEM} and finite differences in Ω_{FDM} . At the top and bottom boundaries of Ω we use first-order absorbing boundary conditions [6]. At the lateral boundaries, mirror boundary conditions allow us to assume an infinite space-periodic structure in the lateral direction.

For simplicity, we assume that $\epsilon = 1$ in Ω_{FDM} . Thus, we only need to reconstruct the electric permittivity ϵ in Ω_{FEM} .

First, we present tests where we reconstruct the parameter ϵ inside the domains Ω_l and Ω_h , see Fig. 3-a), b), respectively. Then we present results from the reconstruction of the structure given in Fig. 3-c).

10.1 Example 1

We start to test the adaptive finite element/difference method on the reconstruction of the structures given in Fig. 3a) and 3 b), where our goal is to find the parameter ϵ in the domains Ω_l and Ω_h , respectively.

To generate data at the observation points, we solve the forward problem (3)-(4) with a plane wave pulse given as

$$\partial_n E|_{\Gamma_1} = ((\sin(\omega t - \pi/2) + 1)/10), \quad 0 \leq t \leq \frac{2\pi}{\omega} = t_1. \quad (34)$$

The field initiates at the boundary Γ_1 , in our examples this boundary represents the top boundary of the computational domain, and propagates in normal direction n into Ω . The trace of the forward problem is measured at the observation points, placed on the lower boundary of the computational domain Ω_{FEM} . On $\Gamma_1 \times (t_1, T]$ and $\Gamma_2 \times (0, T]$ we use first order absorbing boundary conditions, [6]. Here, $T = 10.0$ and the exact value of the parameter is $\epsilon = 4.0$ inside the square lattices and $\epsilon = 1.0$ everywhere else. Since an explicit scheme, [3], is used to solve the forward and adjoint problems, we choose a time step τ according to the Courant-Friedrich's-Levy (CFL) stability condition to provide a stable time discretization.

We start Algorithm 1 in Section 9 with initial guess for the parameter being $\epsilon = 1.0$ at all points in the computational domain Ω_{FEM} and with regularization parameter $\gamma = 0.1$.

To reconstruct the lower and upper squares in Ω_{FEM} , computations were performed on the four adaptively refined meshes shown in Fig. 5-a)-d) and Fig. 6-a)-d), respectively. The meshes was refined by computing the residual in the reconstructed parameter ϵ using Algorithm 1.

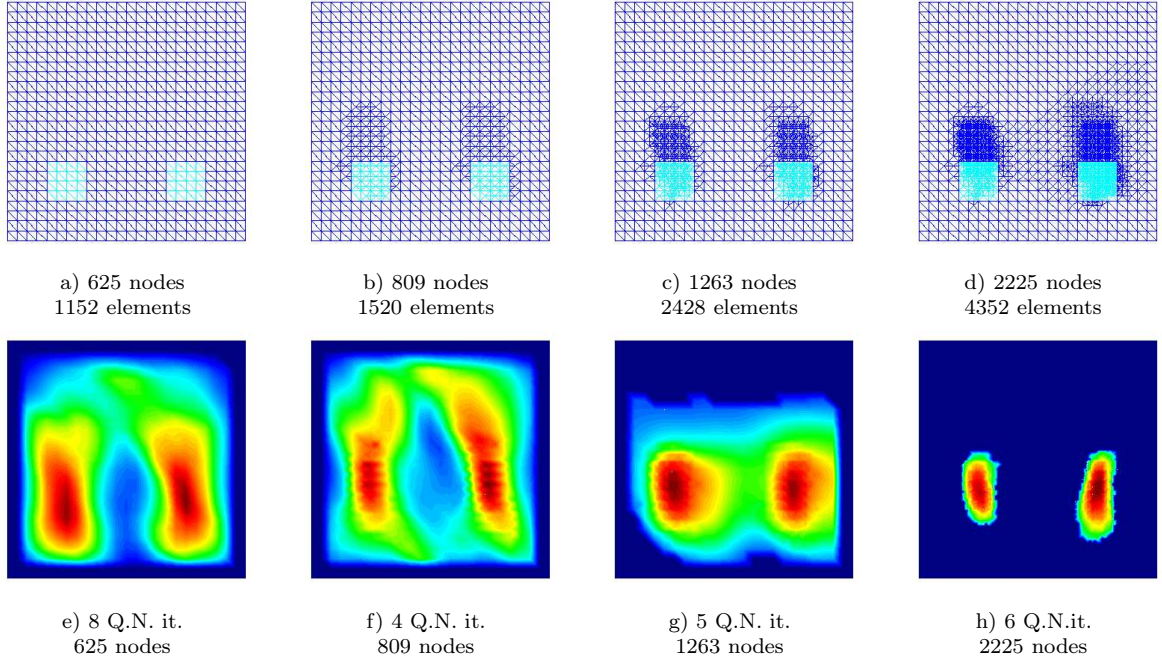


Figure 5: a)-d) Adaptively refined meshes in the reconstruction of the lower square lattices; e)-h) Reconstructed parameter $\epsilon(x)$ on the correspondingly refined meshes at the final optimization iteration computed with $\omega = 25$ and noise level 5% in the observed data.

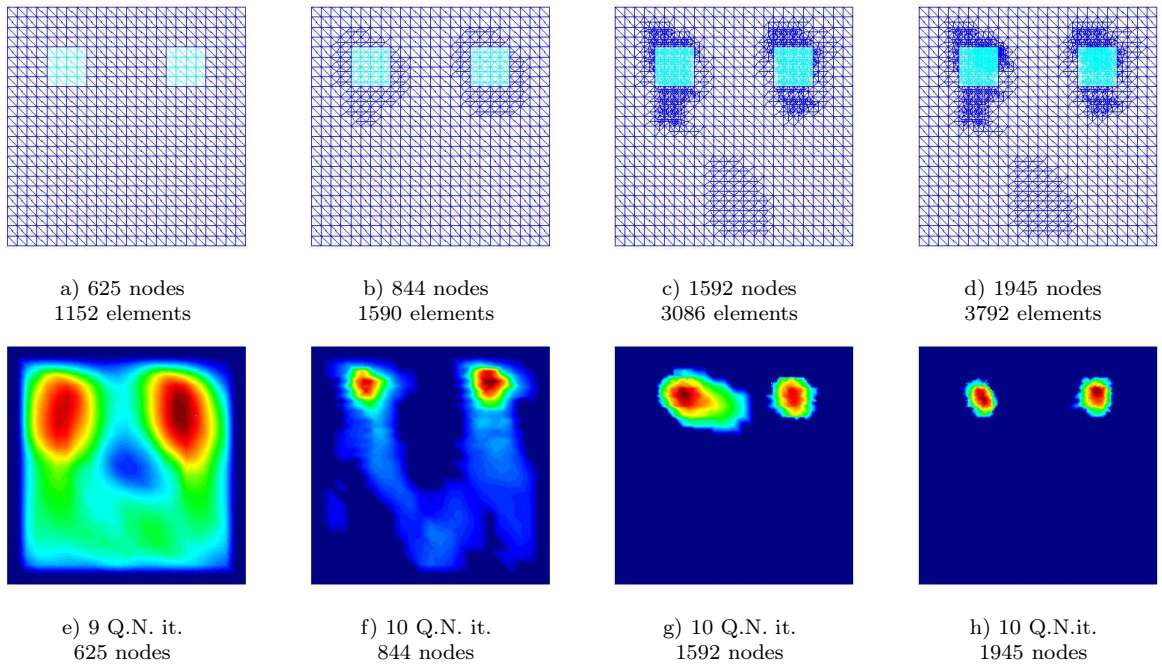


Figure 6: a)-d) Adaptively refined meshes in the reconstruction of the upper square lattices; e)-h) Reconstructed parameter $\epsilon(x)$ on the correspondingly refined meshes at the final optimization iteration computed with $\omega = 25$ and noise level 5% in the observed data.

σ, γ	10^{-5}	10^{-4}	10^{-3}	10^{-2}	10^{-1}
0	0.00630036	0.00630536	0.00475773	0.0046071	0.00313069
1	0.00650122	0.00642409	0.00489691	0.00425432	0.00317147
3	0.00671315	0.00644934	0.00572624	0.00427946	0.00317955
5	0.0068622	0.00661597	0.00639352	0.00428971	0.00318703
7	0.00731985	0.00598225	0.00631647	0.00462458	0.00312281
10	0.00672832	0.00618862	0.00673036	0.00467998	0.00331152
20	0.00702925	0.00696454	0.00640261	0.00448304	0.0037926

Table 2: $\|E - E_{obs}\|_{L_2}$ for the best reconstruction of the lower squares. We present results for the different noise levels σ and regularization parameters γ .

σ, γ	10^{-5}	10^{-4}	10^{-3}	10^{-2}	10^{-1}
0	0.00548847	0.00549544	0.00549544	0.00512397	0.00340977
1	0.00547518	0.00549755	0.00489691	0.0055677	0.00345097
3	0.00545709	0.00550747	0.00572624	0.0055182	0.0040041
5	0.00548414	0.00548424	0.00639352	0.0055076	0.00357293
7	0.00544183	0.00544645	0.00631647	0.00552189	0.00353966
10	0.00543398	0.00548045	0.00673036	0.00552947	0.00430008
20	0.00561054	0.00561999	0.00640261	0.00566159	0.00386997

Table 3: $\|E - E_{obs}\|_{L_2}$ for the best reconstruction of the upper squares. We present results for the different noise levels σ and regularization parameters γ .

Table 1 shows the computed L_2 -norms of $E - E_{obs}$ for the best reconstruction of the parameter ϵ in the lower squares, with $\omega = 25$ in (34). We present the norms on the different adaptively refined meshes at each optimization iteration as long as the norms decrease. The computational tests show that the best results are obtained on the finest mesh, where $\|E - E_{obs}\|_{L_2}$ is reduced by approximately a factor of four between the first and last optimization iterations.

We performed the tests again, adding relative noise to the observed data. The data with relative disturbance, or noise, E_σ , is computed by adding a relative error to the computed data E_{obs} using the expression

$$E_\sigma = E_{obs} + \alpha(E_{max} - E_{min})\sigma/100. \quad (35)$$

Here, α is a random number on the interval $[-1; 1]$, E_{max} and E_{min} are the maximal and minimal values of the computed data E_{obs} , and σ is the noise in percents.

Using the results in Tables 2 and 3 we can conclude that we still have a good reconstruction of the parameter ϵ , when noise is added. These results are confirmed in Fig. 5-e)-h) and Fig. 6-e)-h) where we show the parameter field $\epsilon(x)$, at the final optimization iteration, computed with $\omega = 25$ and noise level 5% in the observed data. We see that although the qualitative reconstruction on the coarse grid already allows the recovery of the location of the squares from the limited boundary data, the quantitative reconstruction becomes acceptable only on the refined grids.

Fig. 7 presents the different L_2 -norms in space of the reconstruction of the lower squares of the adjoint problem solution λ_h over the time interval $(0, 10.0]$. We show the norms in the different optimization iterations on the mesh with 2225 nodes without and with adding 7% noise in the data. We observe that the norms decrease with an increasing number of optimization iterations as it should. We also note that the behavior of the adjoint problem solution is stable to small perturbations in the data. Fig. 8 shows the similar results for the reconstruction of the upper squares.

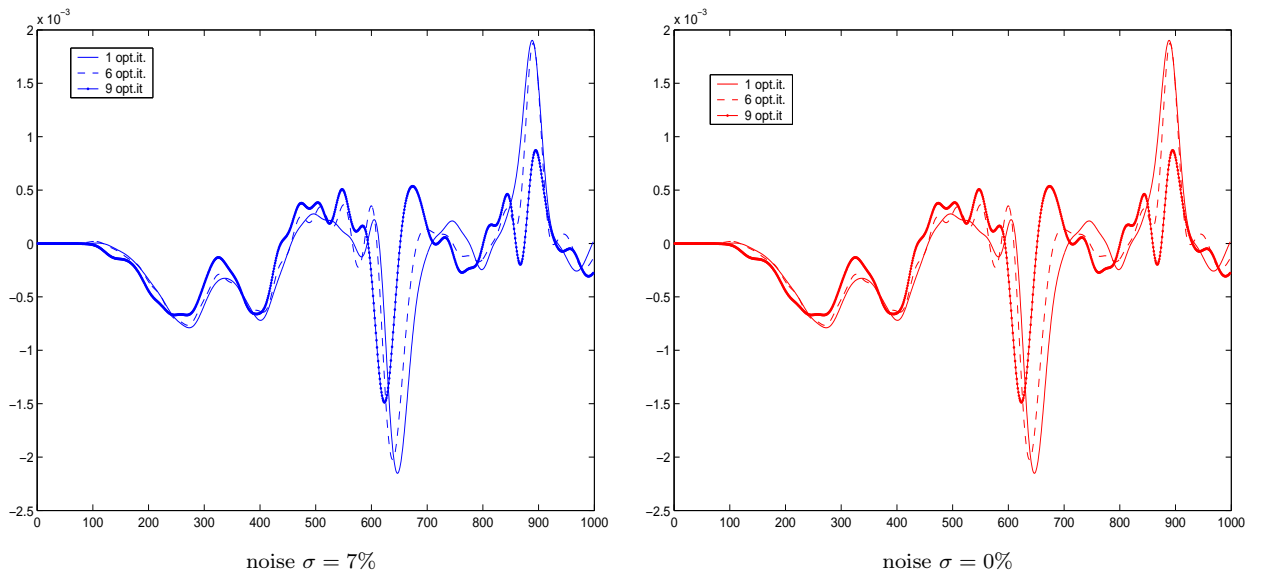


Figure 7: L_2 -norms in space of the adjoint problem solution λ_h in reconstruction of the lower columns in square lattice on different optimization iterations. Here the x -axis denotes time steps on $(0, 10.0)$.

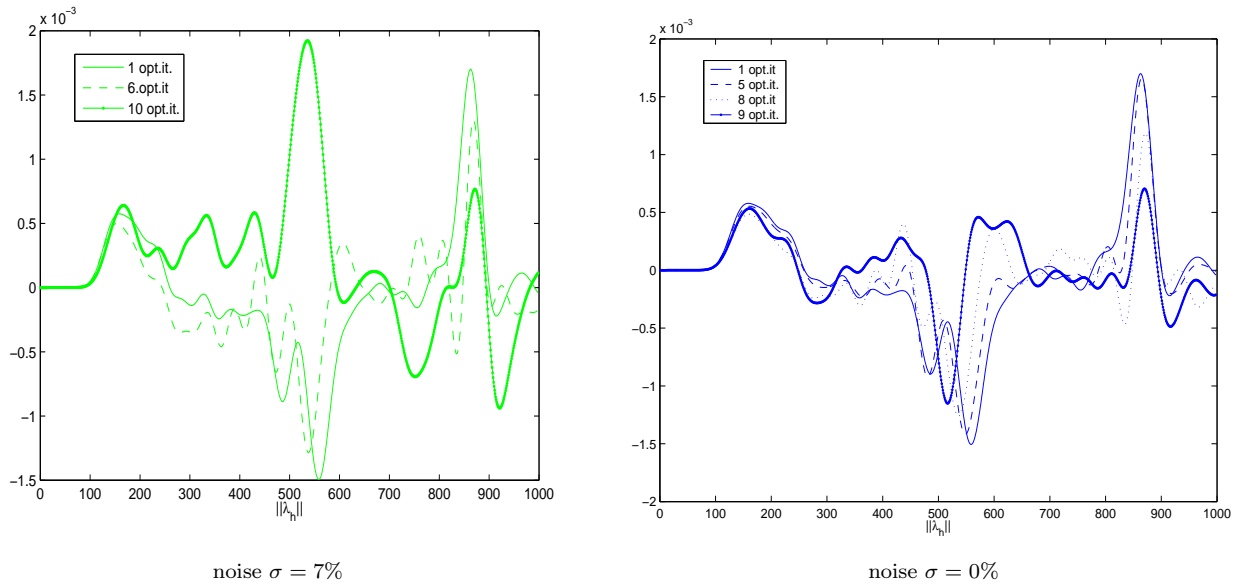


Figure 8: L_2 -norms in space of the adjoint problem solution λ_h in the reconstruction of the upper columns in the square lattice on different optimization iterations. Here the x -axis denotes time steps on $(0, 10.0)$.

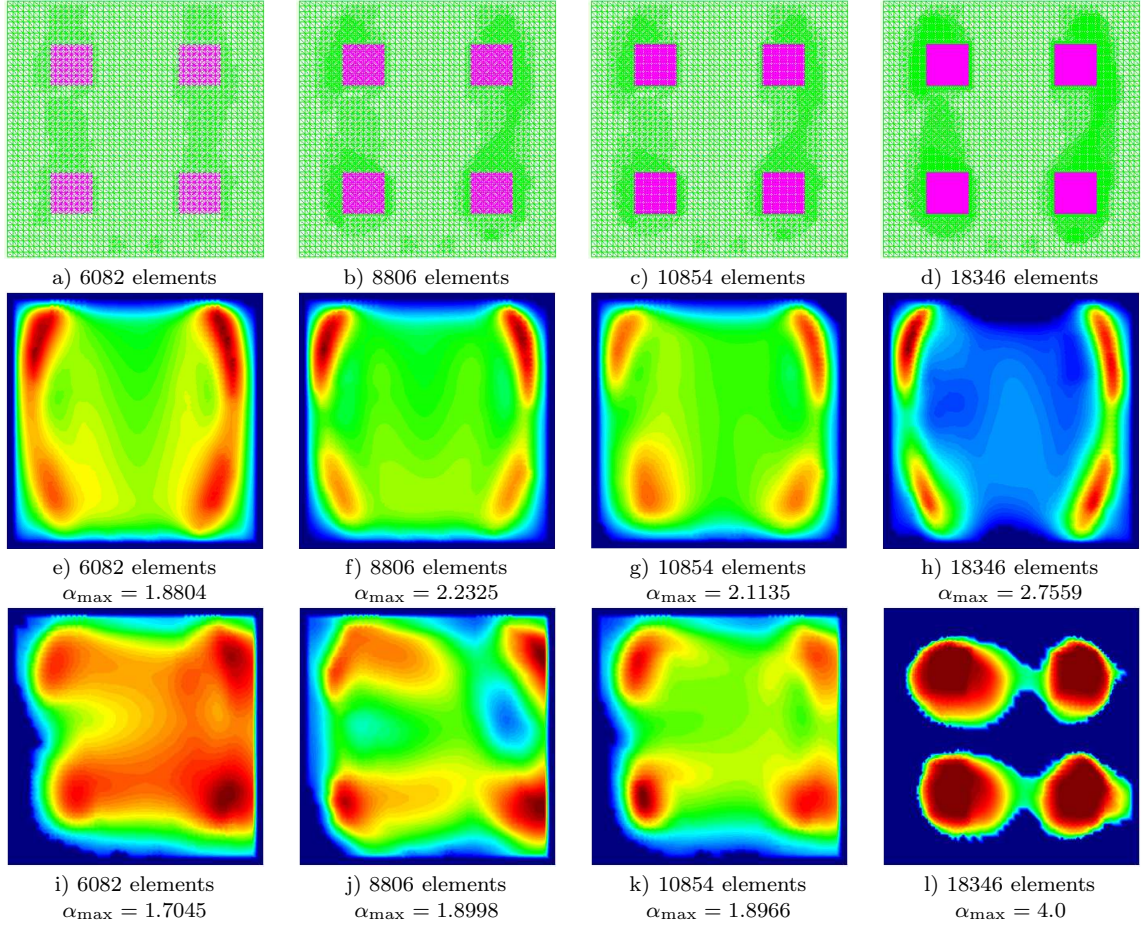


Figure 9: a)-d) Adaptively refined meshes ; Reconstructed parameter $\epsilon(x)$, indicating domains with a given parameter value: e)-h) in Test 1, i)-l) in Test 2. Here, red color corresponds to the maximum parameter value on the corresponding meshes, and blue color - to the minimum.

10.2 Example 2

Now we seek to reconstruct the structure of the two-dimensional crystal given in Fig. 3-c). The electric field (34) initiates at the top boundary of the computational domain Ω_{FDM} and propagates in normal direction n into Ω , with $\omega = 6$. As in Example 1, we use first order boundary conditions on $\Gamma_1 \times (t_1, T]$ and $\Gamma_2 \times (0, T]$.

First we performed tests where the trace of the forward problem is measured at observation points only on the lower boundary, and then, tests where the reflected trace is measured both on the lower and top boundaries of the computational domain Ω_{FEM} .

To achieve better results in the reconstruction, we performed tests letting the incoming wave from the top boundary of Ω_{FDM} be equal to the reflected non-plane wave measured on the lower boundary of Ω_{FDM} . Thus, to generate data at the observation points, we first solve the forward problem (3)-(4) with a plane wave (34) in the time interval $t = (0, T]$ with the exact value of the parameter being $\epsilon = 4.0$ inside the square lattices and $\epsilon = 1.0$ everywhere else, and registered the values of the solution of the forward problem at the lower boundary of Ω_{FDM} . Then, using these registered values, a non-plane wave is initialized, starting at $t = T$ and ending at $t = 2T$. Again, a time step τ is chosen according to CFL stability condition.

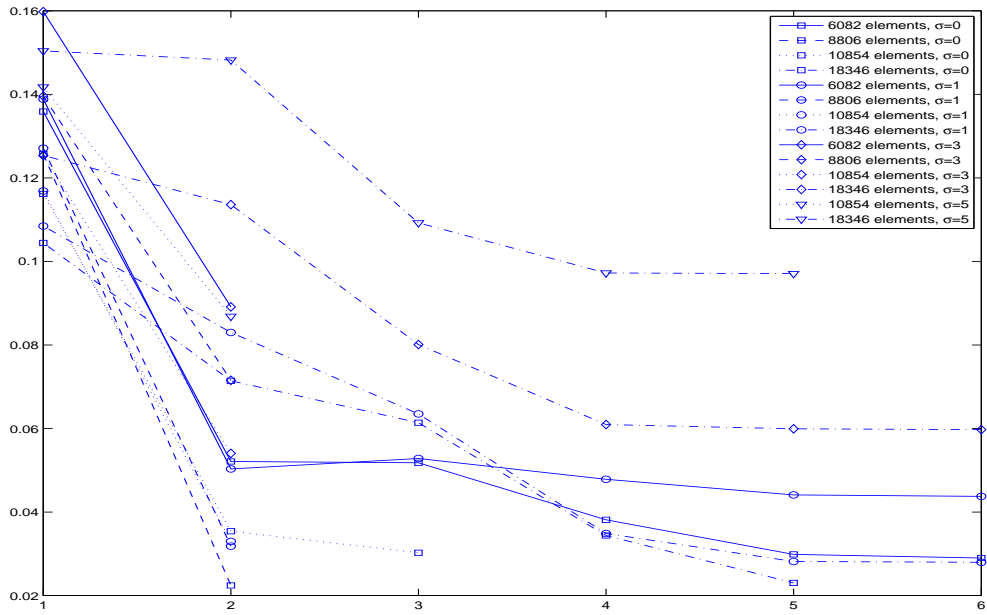


Figure 10: $\|E - E_{obs}\|$ on adaptively refined meshes. Computations was performed with noise level $\sigma = 0, 1, 3$ and 5% and with regularization parameter $\gamma = 0.01$. Here the x -axis denotes number of optimization iterations.

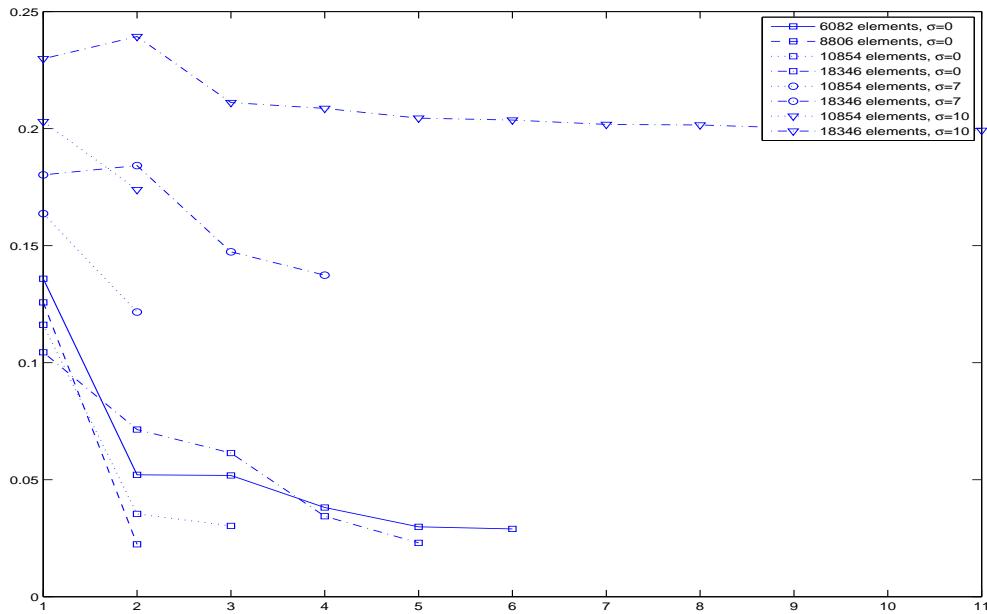


Figure 11: $\|E - E_{obs}\|$ on adaptively refined meshes. Computations was performed with noise level $\sigma = 0, 7$ and 10% and with regularization parameter $\gamma = 0.01$. Here the x -axis denotes number of optimization iterations.

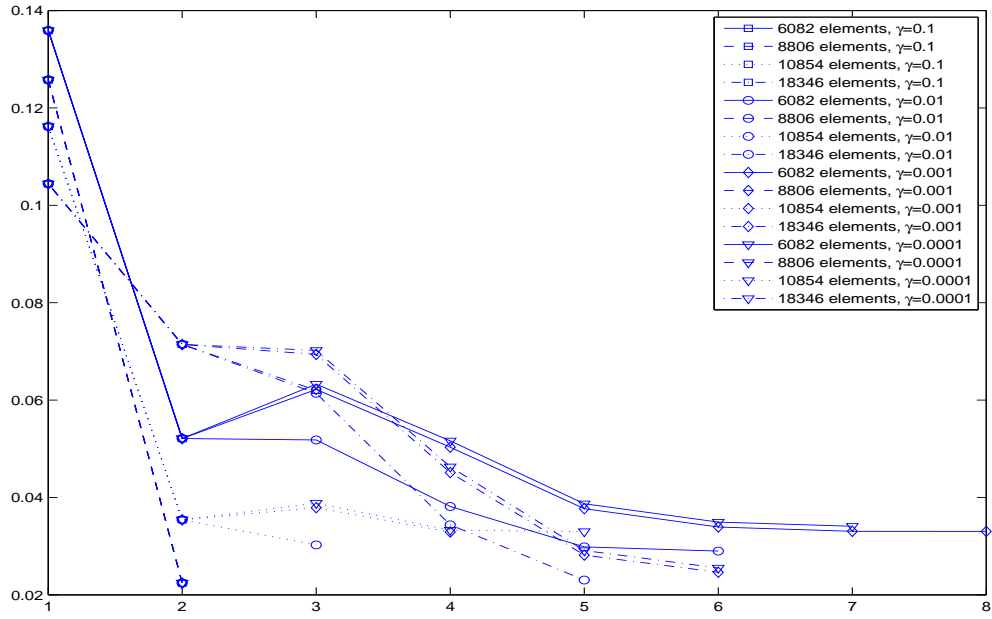


Figure 12: $\|E - E_{obs}\|$ on adaptively refined meshes. Computations was performed with noise level $\sigma = 0\%$, and with regularization parameters $\gamma = 0.1, 0.01, 0.001, 0.0001$, Here the x -axis denotes number of optimization iterations.

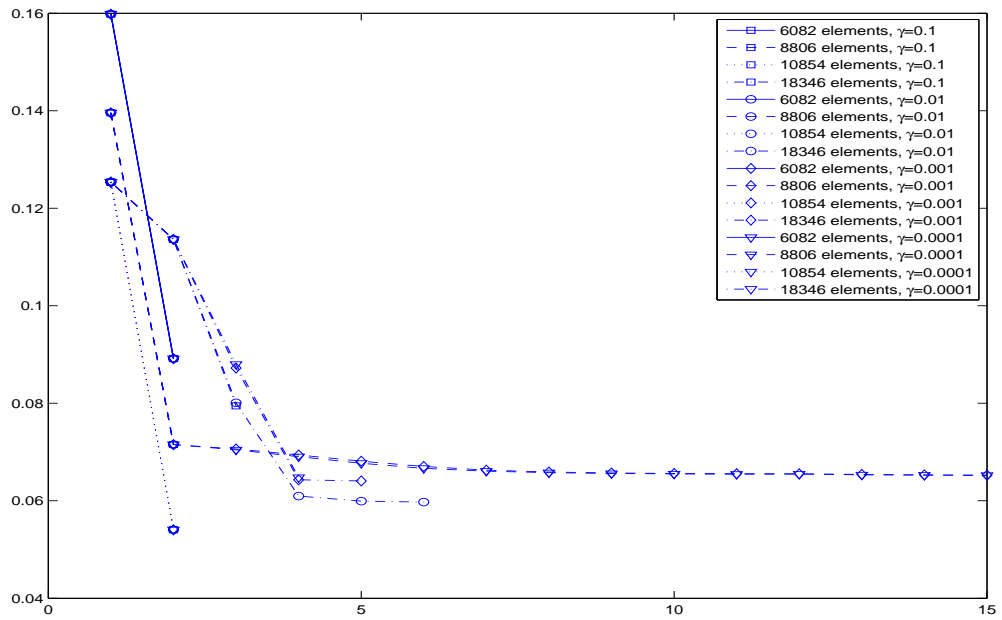


Figure 13: $\|E - E_{obs}\|$ on adaptively refined meshes. Computations was performed with noise level $\sigma = 3\%$, and with regularization parameters $\gamma = 0.1, 0.01, 0.001, 0.0001$, Here the x -axis denotes number of optimization iterations.

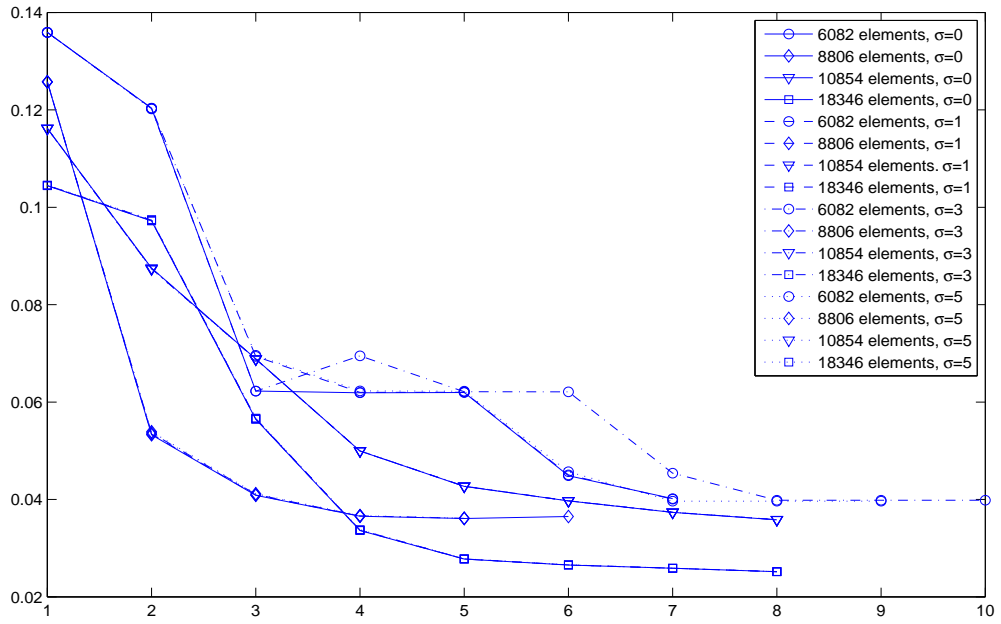


Figure 14: $\|E - E_{obs}\|$ on adaptively refined meshes. Computations was performed with noise level $\sigma = 0, 1, 3$ and 5% and with regularization parameter $\gamma = 0.01$. Here the x -axis denotes number of optimization iterations.

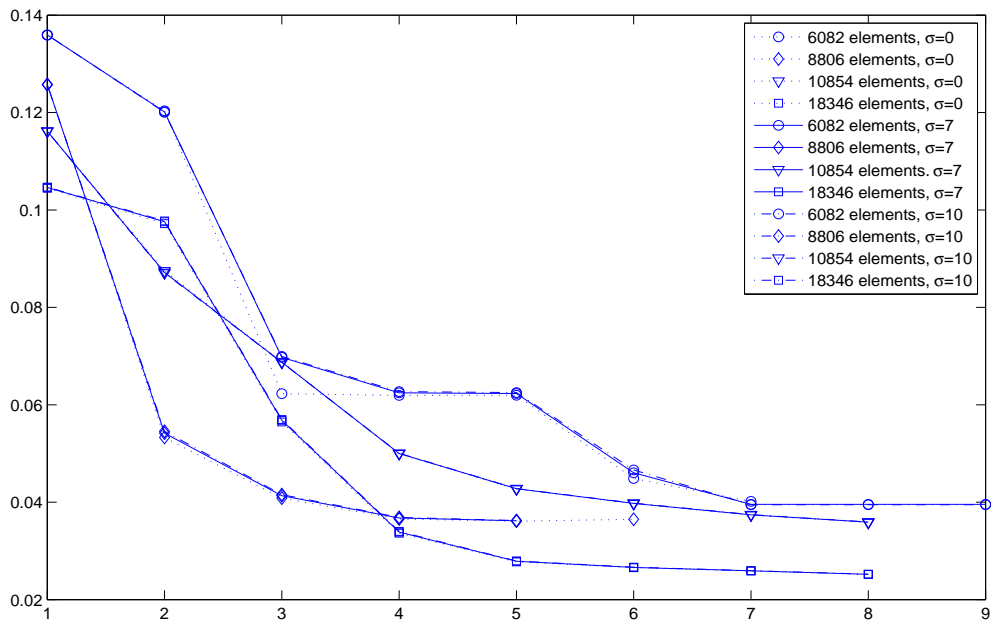


Figure 15: $\|E - E_{obs}\|$ on adaptively refined meshes. Computations was performed with noise level $\sigma = 0, 7$ and 10% and with regularization parameter $\gamma = 0.01$. Here the x -axis denotes number of optimization iterations.

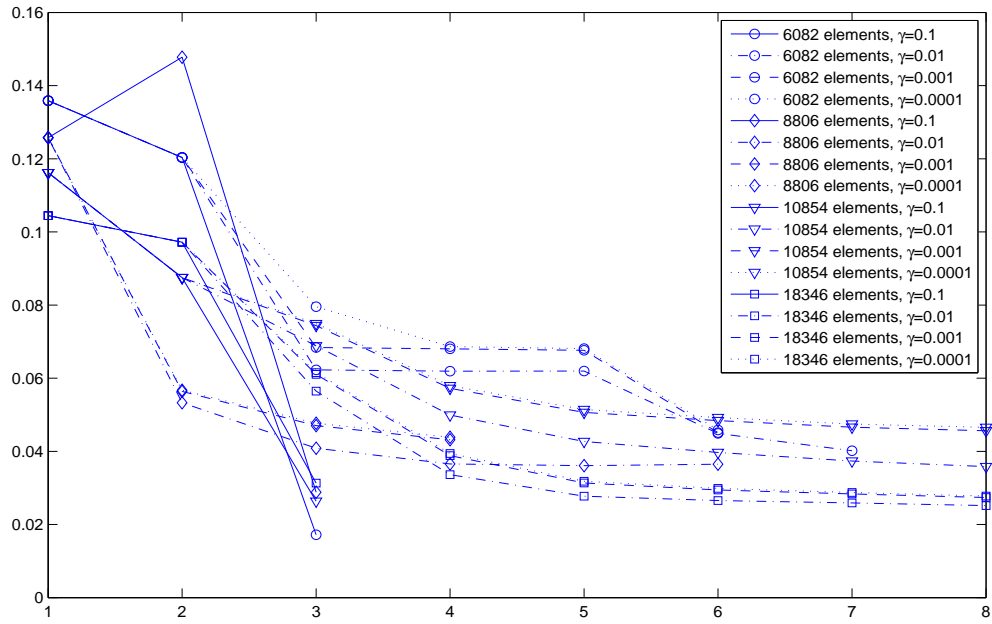


Figure 16: $\|E - E_{obs}\|$ on adaptively refined meshes. We show computational results with noise level $\sigma = 1\%$ and with regularization parameters $\gamma = 0.1, 0.01, 0.001, 0.0001$. Here the x -axis denotes number of optimization iterations.

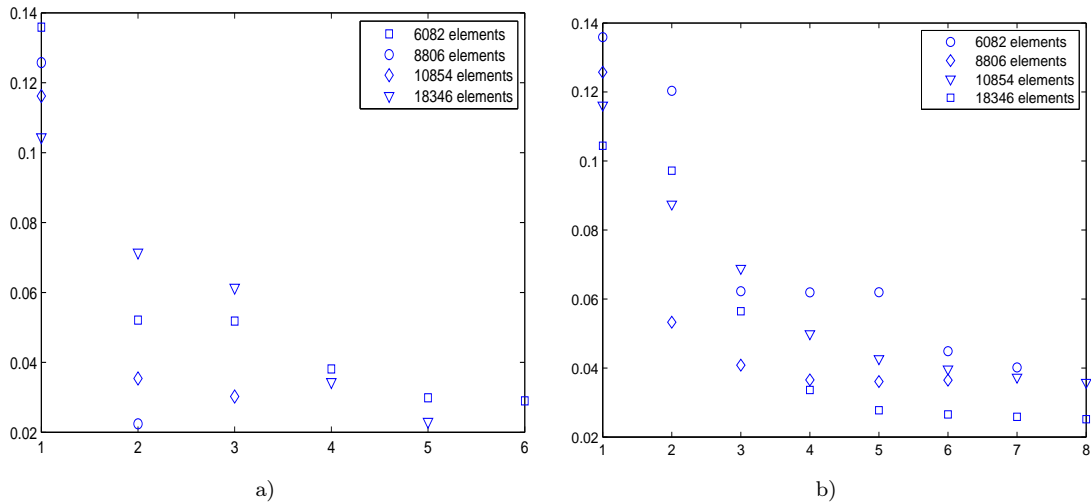


Figure 17: $\|E - E_{obs}\|$ on adaptively refined meshes. We show computations: on a) with noise level $\sigma = 0\%$ and with regularization parameter $\gamma = 0.01$ for Test 1; on b) with noise level $\sigma = 1\%$ and with regularization parameter $\gamma = 0.01$ for Test 2. Here the x -axis denotes number of optimization iterations.

10.2.1 Test1

First we performed the tests where the trace of the incoming wave was measured at the observation points at the lower boundary of Ω_{FEM} in the time interval $(0, T]$, and then at the observation points at the top boundary in the time interval $(T, 2T]$.

In Fig. 10-11 we present a comparison of the computed L_2 -norms, $\|E - E_{obs}\|_{L_2}$, depending on the relative noise σ on the different adaptively refined meshes. The norms are plotted as long as they decrease. The relative noise σ in the data is computed using expression (35). From these results we conclude that the reconstruction is stable with small values of the noise (see Fig. 10), and unstable when adding more than 5% noise to the data (Fig. 11).

In Fig. 12-13 we show a comparison of the computed L_2 -norms, $\|E - E_{obs}\|_{L_2}$, depending on the different regularization parameters γ . We see that we obtain the smallest value of $\|E - E_{obs}\|_{L_2}$ with the regularization parameter $\gamma = 0.01$, while choosing $\gamma = 0.1$ is too large and involve too much regularization. The computational tests show that the best results are obtained on the finest mesh, where $\|E - E_{obs}\|_{L_2}$ is reduced by approximately a factor of seven between the first and last optimization iterations. Fig. 9-e)-h) correspond to Fig. 17-a) and show the reconstructed parameter field $\epsilon(x)$ at the final optimization iteration.

10.2.2 Test2

The tests described in this section, was performed by measuring the trace of the incoming wave at the observation points on both the lower and upper boundaries of the computational domain Ω_{FEM} . Thus, we have twice as much information than in the previous test, and we expect to get a more quantitative reconstruction of the structure.

In Fig. 14-15 we present a comparison of the computed L_2 -norms, $\|E - E_{obs}\|_{L_2}$, depending on the relative noise σ on the different adaptively refined meshes. The norms are plotted as long as they decrease. The relative noise, σ , in the data is computed using expression (35). From these results we conclude that the reconstruction is stable on the two, three and four times refined meshes, even when 10% noise is added to the data.

In Fig. 16 we show a comparison of the computed L_2 -norms, $\|E - E_{obs}\|_{L_2}$, depending on the different regularization parameters γ . We see that the smallest value of $\|E - E_{obs}\|_{L_2}$ is obtained with regularization parameter $\gamma = 0.01$, while $\gamma = 0.1$ is again too large and involve too much regularization. The computational tests show that the best results are obtained on the finest mesh, where $\|E - E_{obs}\|_{L_2}$ is reduced by approximately a factor of seven between the first and last optimization iterations, see Fig. 17-b). Fig. 9-i)-l) correspond to Fig. 17-b), and show the reconstructed parameter field $\epsilon(x)$ at the final optimization iteration.

11 Conclusions and Remarks

We have devised an explicit, adaptive hybrid FEM/FDM method for inverse electromagnetic scattering. The method is hybrid in the sense that different numerical methods, finite elements and finite differences, are used in different parts of the computational domain. We derived an a posteriori estimate for the error in the Lagrangian in the case when we have first order absorbing [6] and mirror boundary conditions in the formulation of the forward problem. The adaptivity is based on a posteriori error estimates for the associated Lagrangian in the form of space-time integrals of the residuals multiplied by the dual weights. In future work we plan to determine the error in the reconstructed parameter

numerically, by solving an associated problem for the Hessian of the Lagrangian. We illustrated the usefulness of the adaptive error control on an inverse scattering problem for recovering the electric permittivity from boundary measured data.

References

- [1] R. Becker. Adaptive finite elements for optimal control problems. *Habilitationsschrift*, 2001.
- [2] R. Becker and R. Rannacher. An optimal control approach to a posteriori error estimation in finite element methods. *Acta Numerica*, Cambridge University Press, pages 1–225, 2001.
- [3] L. Beilina. *Adaptive finite element/difference methods for time-dependent inverse scattering problems*. PhD thesis, Department of Computational Mathematics, Chalmers University of Technology, 2003.
- [4] L. Beilina and C. Johnson. A posteriori error estimation in computational inverse scattering. *J. Mathematical models and methods in applied sciences*, 15(1):23–37, 2005.
- [5] L. Beilina, K. Samuelsson, and K. Åhlander. Efficiency of a hybrid method for the wave equation. In *International Conference on Finite Element Methods*, Gakuto International Series Mathematical Sciences and Applications. Gakkotosho CO.,LTD, 2001.
- [6] B. Engquist and A. Majda. Absorbing boundary conditions for the numerical simulation of waves. *Math. Comp.*, 31:629–651, 1977.
- [7] K. Eriksson, D. Estep, and C. Johnson. *Computational Differential Equations*. Studentlitteratur, Lund, 1996.
- [8] J. Nocedal. Updating quasi-newton matrices with limited storage. *J. Mathematical of Comp.*, 35, N.151:773–782, 1991.
- [9] O. Pironneau. *Optimal shape design for elliptic systems*. Springer Verlag, Berlin, 1984.